NTNU – Trondheim
Norwegian University of
Science and Technology

Development of Signal Processing Tools and Analysis of Hyperspectral Imaging Data in Diagnostics of Prion Diseases

Thomas Trøen

Teacher Education with Master of Science
Submission date: June 2013
Supervisor: Mikael Lindgren, IFY

Norwegian University of Science and Technology
Department of Physics

Abstract

Creutzfeld-Jakob disease is an invariably deadly prion disease with no cure that attacks the brain. Hyperspectral microscopy has been used to examine 26 amyloid plaques (captured with two different filters) present in infected brains, stained with the luminescent polymer hFTAA. A MatLab program using the correlation coefficient between the emission spectrum from the sample and a reference spectrum representing the autofluorescence from the center of a plaque is used to examine where the staining is most evident. The correlation proved to be highest at the periphery of the plaques, indicating that the staining was most pronounced in the center. Two new programs were written to view the emission spectra for different distances from the center. The first program used pixels in the hyperspectral image lying on five circles with different radius, while the other used pixels from intensity based zones in the image. As it proved to be the most reliable, the latter was preferred used on the hyperspectral images in the data set. A distinct red shift in emission spectra as one moves from the periphery to the center of the plaques was revealed, as well as a strong increase of intensity and at around 606 nm.

Sammendrag

Creutzfeld-Jakobs sykdom er en kurløs og alltid dødelig prionsykdom som angriper hjernen. Hyperspektral mikroskopi har blitt brukt til å undersøke 26 amyloideplakk (tatt opp med to forskjellige filtre) tilstede i infiserte hjerner som er markert med hFTAA. Et MatLab-program som bruker korrelasjonskoeffisienten mellom prøvens emitterte spekter og et referansespekter som representerte autoflourescensen har blitt brukt til undersøke hvor markeringen er mest synlig. Korrelasjonen viste seg å være høyest ved periferien av plakkene, hvilket indikerer at markeringen var sterkest i senteret. To nye program ble skrevet for å undersøke hvordan det de emitterte spekterne så ut for forskjellige avstander fra senteret. Det første programmet brukte pixler i det hyperspektrale bildet som lå på fem sirkler med forskjellig radius, mens det andre brukte pixler fra soner i bildet inndelt på bakgrunn av intensitet. Den sonebaserte teknikken viste seg være den mest pålitelige, og ble derfor foretrukket for bruk til videre analyse på de hyperspektrale bildene i datasettet. Analysen viste en tydelig rødforskyvning for de emitterte spekterne når man gikk fra periferien til sentrum av plakkene, og en sterk økning i intensitet ved omlag 606 nm.

Preface

This master's report is a result of data gathered within the LUPAS project (Luminescent Polymers for in vivo imaging of Amyloid Signatures) terminated in Dec 2012. It represents the course FY 3950 with 30 credits.

I would like to thank Pål Gunnar Ellingsen, my guide for the technical details and programming, and professor Mikael Lindgren for providing good feedback in discussing results and drafting the report.

A thanks also goes out to collaborating partners in Zürich for good information about the experimental setup and for providing data. The groups of Prof Hammarström and Nilsson in Linköping are acknowledged for good background information about the research previously done regarding the subject.

Thomas Trøen
June 1, 2013

Table of Contents

List of Tables

List of Figures

Abbreviations

PrP^{C}	=	The prion protein existing in the membrane of cells.
PrP^{Sc}	=	Misfolded form of the prion protein
CJD	=	Creutzfeldt-Jakob Disease
sCJD	=	CJD obtained sporadic
AD	=	Alzheimers disease
M and V	=	Methionine and Valine
BBB	=	the Blood Brain Barrier
hFTAA	=	heptamer Formyl Thiophene Acetic Acid
AF	=	Autofluorescence
FP7	=	7 th Framework Programme for Research and Technological Development.
LUPAS	=	Luminescent Polymers for in vivo imaging of Amyloid Signatures. It is a EU-project within FP7.

Chapter 1

Introduction

1.1 Microscopy

Microscopy is about taking advantage of object properties such as reflection and absorption, and making them visible in a way not possible by using only the naked eye. Classical optical microscopes forms an image of the object examined using glass lenses to focus light onto the eye. Although the invention of the microscope is dated to the late 1500s [11], new techniques are still being developed. Mostly, novel techniques make use of fluorescence, a phenomenon first discovered by Sir George Gabriel Stokes in 1852. Fluorescent molecules serve as a light source found in specific locations of a specimen, pointing out their position by emitting light with a characteristic spectrum. The energy required to emit this light is obtained by the molecule through the excitation light, which in a microscope is provided by the light source (see figure 1.1). There are two ways to make use of fluorescent microscopy, and the object being investigated is decisive for how it is used. The object it self could be fluorescent, or fluorochromes are added to the object [2].

1.1.1 Autofluorescence

Autofluorescence (AF) is natural fluorescence by biological objects, and is widely found in nature. Fluorochromes may also be added to objects having a significant amount of AF. Thus, it is necessary to separate AF from the desired fluorochrome emission. Uptil now, there have not been any good methods to do that since fluorescence is traditionally is collected in one or a few wavelength channels, governed by special filter settings. With the advance of spectrally resolved images one gets new possibilities to analyze data in a refined way.

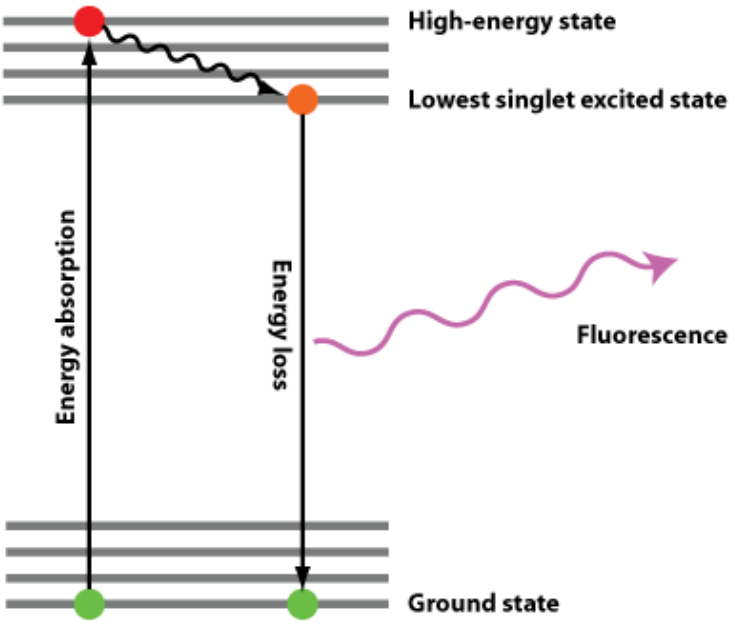

Figure 1.1: A Jablonski diagram illustrating the process of fluorescence. An electron is excited from the ground state to a higher energy state by absorption of excitation light. The electron then goes back to the ground state and releases the excess energy as a photon, known as fluorescence. The fluorescenct light wavelength will be longer than the excitation light wavelength, as some energy is lost to vibrational heat in the high energy state. Figure from scienceinyoureyes.com [7].

1.2 Hyperspectral imaging

Hyperspectral imaging is a branch of spectral imaging that has very high spectral resolution. High resolution here means a few nm in the visible range, which is a major improvment over previous few channel wavelength separation. The technique combines spectroscopy with regular imaging, which results in a lot of information being saved in one dataset, see figure 1.2 [5, 29].

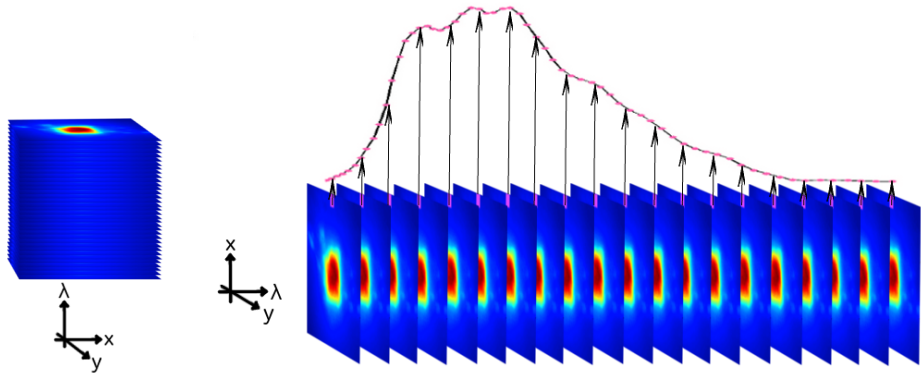

(a) A hyperspectral cube.

(b) The spectrum from one pixel can be extracted form a hyperspectral image.

Figure 1.2: Every pixel in a hyperspectral image carries information about intensity distribution per wavelength. The intensity, I, of a spectrum is mathematically described as dependent on the wavelength λ, $I(\lambda)$, while a regular intensity image depend on the spatial coordinates x and y, $I(x, y)$. A hyperspectral image can therefore be represented as a three dimensional image, $I(x, y, \lambda)$, often visualized as the cube in (a). As shown in (b), the spectrum can be extracted from every pixel in the image and will be limited by the spectral resolution (i.e. the number of images in the cube). The colors of the images in this figure is related to the intensity.

1.2.1 Signal processing

Hyperspectral images can be analyzed more or less detailed based on what application one is aiming for, as well as the nature of the object that may contain much AF background signal. One could for example focus on what the emission spectrum from an image looks like, or how the spectrum from every pixel is [8]. A classic situation in signal processing of hyperspectral images is when a spectrum originates from many different sources, some not as wanted as others. This can for example be the Poisson noise of the fluorescence signal, or simply noise originating from the detector. A technique called linear unmixing has been developed to separate and give a relative weighting to the spectra present in a spectrum, given that there exists a reference spectrum for each spectra that is present. Linear unmixing has proven to be effectful to reduce noise, as well as being able to separate spectra from an object stained with more than one fluorochrome if signal to noise is high enough [29].

Another quite similar technique is based on calculating the correlation coefficient between an emitted spectrum and a reference spectrum. The technique does not assume anything about the sample, and have been used on other applications having a low signal to noise ratio. As hyperspectral images can contain a lot of noise due to the large amount of wavelength channels, the correlation approach is a suiting technique for that purpose [4].

1.3 Applications

1.3.1 Prion diseases

In this master work the aim is to develop signal processing tools for bioimaging. Specifically, we are interested in neurological diseases based on protein disorder. Prion diseases are inevitable fatal neurodegenerative diseases. All types evolves in the same manner - through change in conformation of the prion protein from its common form, PrP^{C}, into the pathogenic amyloid form, PrP^{Sc} [14].

PrP^{Sc}, and therefore prion diseases, can be obtained in three different ways; infectious, inherited and sporadic. The presence of PrP^{Sc} is then the catalyst of the PrP^{C} to PrP^{Sc} conversion [15]. This conversion is believed to occur through refolding of PrP^{C} [20]. Some research suggests that the absence of PrP^{C} due to refolding into PrP^{Sc} is the pathogenic factor [16], although most research labels the isoform PrP^{Sc} as cause for the disease [26]. PrP^{Sc} is enriched with β-sheets, which is structurally more stable than the α-helical fold of PrP^{C} [27, 18], see figure 1.3.

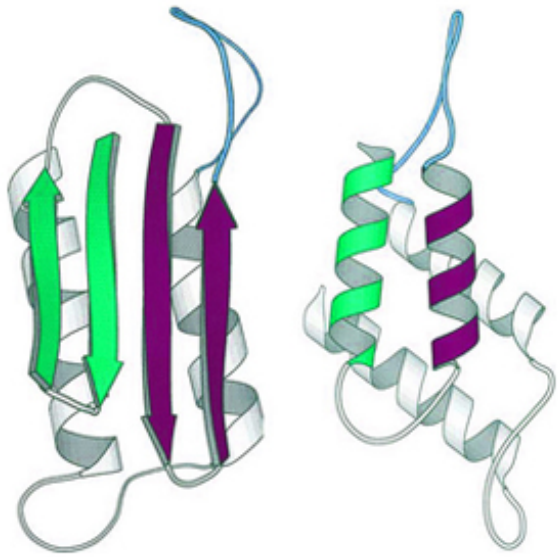

Figure 1.3: Illustration of two different foldings of the prion protein. To the left is the folding with β-sheets, PrP^{Sc}, and to the right is the structurally weaker α-helical fold, PrP^{C}. Conformational change from the α-helical fold to the β-sheets fold is believed to be the pathogenic factor for prion diseases. Figure from learner.org [10]

Creutzfeldt-Jakob disease

Creutzfeldt-Jakob disease (CJD) is a prion disease that can occur to humans, progresses at a high rate, and is as all prion diseases, invariably deadly. There exists two types of PrP^{Sc} emerging in CJD, type 1 and type 2, and the genotype at the polymorphic codon 129 can be M/V, M/M or V/V [1, 17]. This gives a total of six

combinations, although M/M1 and M/V1 has proven to be defiant to distinguish [19]. There has been reported that co-occurence of different types of PrP^{Sc} can happen in one diseased brain [21, 6].

1.4 Staining amyloids

It has been reported that heptamer formyl thiophene acetic acid (hFTAA) passes BBB in mice and stains amyloid-β plaques, and the most significant staining has happened on the periphery of the plaque [25, 3]. Similarly, such stains called LCP (luminescent conjugated polymer) or LCO (luminescent conjugated oligomers) can be used to stain a large variety of protein amyloid states.

1.5 The project objective

In the FP7 EU-project LUPAS a lot of new probes for diagnostics of Alzhheimer's disease (AD) and prion diseases were developed. Here a set of data from human form of CJD is analyzed using the new correlation algorithm. The purpose is to see differences in spectral response for the stain hFTAA in different samples, and to develop new auxiliary help routines to assist in the handling and analysis of data.

Chapter 2

Background and Theory

2.1 Correlation analysis

In order to separate two quite similar emission spectra, correlation analysis has been used with success. A MatLab program named plotCorrelation, developed by Pål Gunnar Ellingsen in the LUPAS-project [4], calculates the correlation between the spectrum in a hyperspectral image pixel and a reference spectrum by using the correlation coefficient (equation 2.2).

$$\rho_{XY} = \frac{\sigma_{XY}}{\sigma_X \sigma_Y} \tag{2.1}$$

X and Y are in equation (2.1) random variables, σ_{XY} is the covariance between X and Y, and σ_X and σ_Y is in accordance with conventional notation the standard deviation of X and Y, respectively. The resulting correlation is in the interval $-1 \leq \rho_{XY} \leq 1$, where 1 means that $X = Y$, and -1 that $X = -Y$. When applied on hyperspectral images, X and Y represents the reference spectrum and the spectrum in a pixel. Assuming N data points gives:

$$\rho_{XY} = \frac{\sum_{i=1}^{N}(X_i - \bar{X})(Y_i - \bar{Y})}{\sqrt{\sum_{i=1}^{N}(X_i - \bar{X})^2}\sqrt{\sum_{i=1}^{N}(Y_i - \bar{Y})^2}} \tag{2.2}$$

where $\bar{X}$ and $\bar{Y}$ represents the mean values of X and Y, respectively [4] An example on application of plotCorrelation is shown in figure 2.1.

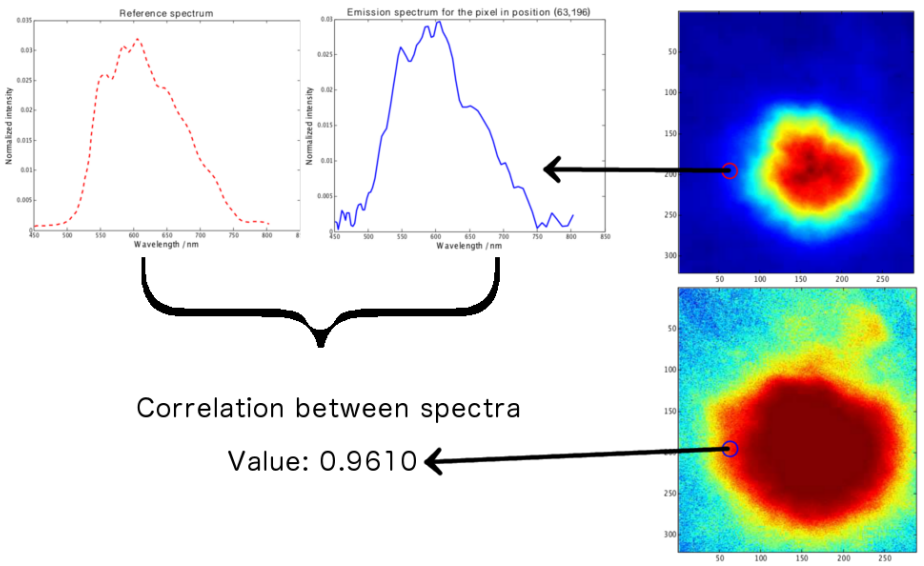

Figure 2.1: The figure illustrates how plotCorrelation is used to find the correlation between a reference spectrum and the emission spectrum for all pixels in a hyperspectral image. The emission spectrum is extracted from the image and its correlation with the reference spectrum is calculated. The resulting value, in this case 0.9610, is plotted in a new figure with the same dimensions as the hyperspectral image at the exact same point, which in this case is at (63,196) (X and Y position respectively). When all correlation coefficients are calculated and plotted, a heat map showing the emission spectra's correlation with the reference spectrum at all points in the hyperspectral image is shown.

2.2 Linear unmixing of emission spectra

Linear unmixing can be used to identify and separate overlapping spectra, for example fluorescence from objects stained with more than one fluorochrome. Mathematically, a measured spectrum can be described as:

$$\mathbf{S}(\lambda) = \sum \mathbf{A}_i * \mathbf{R}_i(\lambda), \tag{2.3}$$

where $\mathbf{R}$ is the reference spectra and $\mathbf{A}$ is a weighting matrix. Solving the equation requires linear algebra [9].

2.3 Statistics

Statistics is essential in the process of handling large amount of data. A mean value with its standard deviation reports about the consistency of the results. When handling multiple emission spectra, a mean spectrum with standard deviation can be calculated to discover common features.

If $X_1, X_2, \ldots, X_n$ is a random sample of size n, the sample mean is defined as (2.4)

$$\bar{X}_n = \frac{1}{n}\sum_{i=1}^{n} X_i \tag{2.4}$$

where $\bar{X}_n$ is mean value and X_i is the value for the i'th element. The sample variance is defined as (2.5)

$$\sigma^2 = \frac{1}{n-1}\sum_{i=1}^{n}(x_i - \bar{x})^2 \tag{2.5}$$

where σ is the standard deviation [24].

2.3.1 The weak law of large numbers

If the random numbers $X_1, X_2, X_3, \ldots$ has mean μ, the mean value, $\bar{X}_n$, for the first n numbers approaches μ as n increases towards infinity. That is, for any positive ϵ:

$$\lim_{n\to\infty} P(|\bar{X}_n - \mu| > \epsilon) = 0, \tag{2.6}$$

where P is the probability [22].

Chapter 3

Method

3.1 Programming

For implementation of new tools to analyze hyperspectral images, the software MatLab [13] was used to make it compatible with previous work from the LUPAS project. For exploring the radial dependence of spectra, two new scripts were written. The first is based on spectra from a fixed distance from a chosen centre in the image, named the circle-method. The other is based on spectra from pixels in image having a total intensity within a certain interval, the zone-method. Pseudo codes are shown in algorithms 1 and 2.

```
Input: Hyperspectral image as 3D matrix, array with wavelength values
Output: Mean emission spectra for points a fixed distance from centre with
        standard deviations
display hyperspectral image in figure;
take user input to define centre and five integer radii;
normalize spectra for every pixel in image with respect to area;
for all radii do
    find positions in hyperspectral image whose distance from centre,
    calculated by the pythagorean theorem and rounded to an integer, is
    equal to radius;
    for all wavelengths do
        find mean value and standard deviation for pixels located at
        calculated positions in hyperspectral matrix;
    end
end
return
```

Algorithm 1: How the emission spectra is calculated in circle-method.

Input: A = Hyperspectral image as 3D matrix,
$wave$ = array with wavelength values
Output: Emission spectra with standard deviations for all zones
$xStep \leftarrow [0.1, 0.2, 0.3, \ldots, 1]$;
$img \leftarrow$ 2D intensity image;
`/* finding max and min value of image: */`
$maxImg \leftarrow max(img)$;
$minImg \leftarrow min(img)$;
`/* all values in` $xStep$ `is used to make an array containing upper intensity limits for the zones */`
$limits \leftarrow xStep * (maxImg - minImg) + minImg$;
for $i \leftarrow 1$ ***to*** 10 **do**
  if $i = 1$ **then**
    $zone_i \leftarrow$ [pixels with intensity value $\leq limits(i)$];
  else if $i = 10$ **then**
    $zone_i \leftarrow$ [pixels with intensity value $> limits(i-1)$];
  else
    $zone_i \leftarrow [limits(i-1) <$ pixels with intensity value $\leq limits(i)]$;
  end
  for $j \leftarrow 1$ ***to*** *length of wave* **do**
    `/* Calculate mean value and standard deviation for pixels in zone`$_i$ `for every wavelength */`
    $zoneSpec(zone_i, wave_j) \leftarrow \text{mean}(A(zone_i, wave_j))$;
    $stdSpec(zone_i, wave_j) \leftarrow \text{std}(A(zone_i, wave_j))$;
  end
end
return *zoneSpec stdSpec*

Algorithm 2: How the emission spectra is calculated in zone-method.

3.2 Pythagorean theorem

To calculate the distance between two pixels in a digital image, the pythagorean theorem is used [23]:

$$d = \sqrt{(X_2 - X_1)^2 + (Y_2 - Y_1)^2}, \tag{3.1}$$

where (X_1, Y_1) and (X_2, Y_2) are the coordinate positions of the two pixels, and d is the distance between them.

3.3 Hyperspectral images in dataset

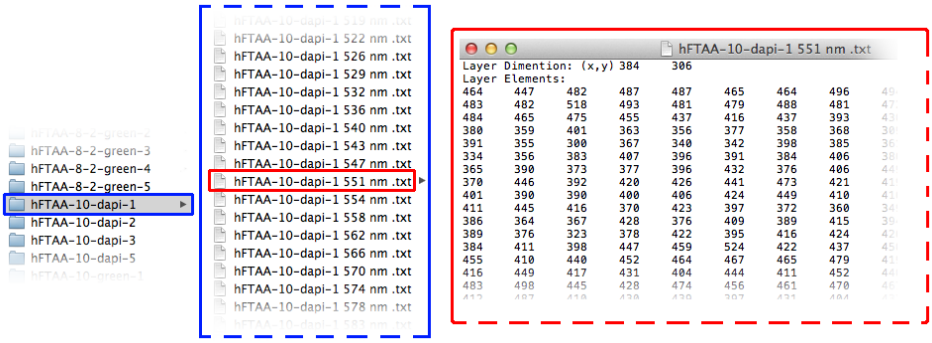

Figure 3.1: The dataset contained 56 folders, one for each hyperspectral image. Every folder contained a set of *.txt files, one for each wavelength (i.e. one for each layer in the hyperspectral image, see figure 1.2). Every *.txt file contained information about how many counts that were registered by the detector at every point.

Figure 3.1 illustrates how the hyperspectral images were saved in *.txt files. A MatLab function called readSpecFiles (written by Pål Gunnar Ellingsen) could take one folder as input, and give a three dimensional matrix and a one dimensional array as output. The matrix can be understood as the hyperspectral cube seen in figure 1.2, where numerical values in the plane constructed by the two first dimensions represents the number of counts registered by the detector, i.e. the intensity. Every step in the third dimension is one layer in the hyperspectral cube. The one dimensional array output is an ordered list of wavelengths corresponding to the layers (wavelengths is extracted from the filename, see figure 3.1).

The images in the dataset had dimensions in the range 208-784 pixels in the X direction and 218-720 pixels in the Y direction. The mean resolution of all images was 372x343. In terms of spectral resolution, all hyperspectral images had a starting wavelength at around 450 nm and ending at around 807 nm. All of them had around 80 files, so that in average, 4-5 nm separated each data point.

3.4 Laboratory work

Laboratory work is performed by Hennig Leske at the university of Zürich. The samples are sections of the cerebellum in human tissue, since it is uncommon to have amyloid-β plaques there, which would be a confounder for this study. All plaques are sporadic CJD (sCJD) cases.

3.4.1 Sample preparation

10 μm thick frozen sections of human tissue were dried at room temperature, fixated using 100% ethanol, and subsequently washed twice using PBS. The following step was staining the sections with hFTAA diluted in PBS for 30 minutes. After that they were washed twice in PBS, dried and sealed using dako fluorescence mounting medium and a coverslip. Nailpolish was applied to prevent NaOH to access the tissue. After hardening of the nail polish (1 day), the sections were decontaminated in 2M NaOH, washed in H2O and analyzed.

3.4.2 Experimental setup

Microscope information is given in table 3.1. The images were collected with a 1000 fold magnification, using Olympus oil. The spectra were calibrated so that there was no more difference than 2 nm according to the reference. Pictures of plaques were taken and the exposure time was set, so that the brightness level of the image was always around 3000 with filter set 1 and filter set 9. Filter set 1 excites with BP 365 nm (FWHM 12 nm), has a beam splitter FT 395 nm and a LP 397 nm filter for emission. Filter set 9 excites with BP 450-490 nm, has a beam splitter FT 510 and a LP 515 nm filter for emission [28].

Microscope:	Zeiss Axioplan 2 Imaging
Filter:	Zeiss filter set 1 and Zeiss filter set 9
Lamp:	HXP 120C

Table 3.1: Microscope information

Chapter 4

Results and discussion

4.1 Normalization of multiple spectra in one plot

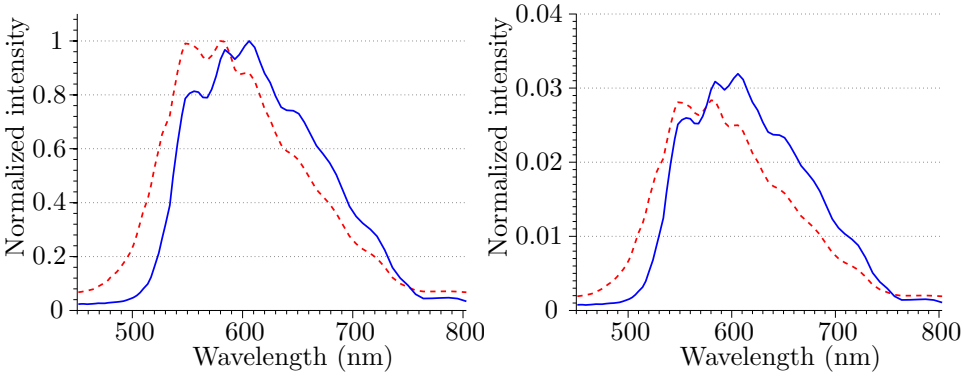

(a) Spectra normalized with respect to maximum value

(b) Spectra normalized with respect to area under curve

Figure 4.1: Illustration of the differences between normalizing spectra with respect to maximum value and area under curve. The area normalization reveals that the blue spectrum (unbroken line) has a larger portion of its total energy at the maximum value compared to the red spectrum (dotted line), which does not show in a spectrum normalized with respect to the maximum value. This is because the area normalization shows how every peak changes its value with respect to the total spectrum. The red shift happening is more evident with area normalizing, and the fact that the peak at 600 nm for the blue (unbroken line) spectrum increases relative to the peak at 550 nm for the red (dotted line) spectrum is much easier to see with area normalization.

For both the zone-method and the circle-method, normalization of the mean spectra is done with respect to area under the curve. In the earlier version of plotCorrelation, normalization was done with respect to maximum value. This is however

the first time multiple spectra is plotted in the same figure in the program, and normalization with respect to maximum value does not give a good visualization of how the spectra changes. Differences between the two is illustrated in figure 4.1.

To normalize the spectra, the MatLab built-in function trapz is used [12]. It uses the trapezoidal rule on the values available for the spectrum (typically around 80 for dapi filtered images, and some fewer for green filtering due to a higher wavelength cut-off). Mathematically speaking, the trapezoidal rule is a simplification of area calculation. However, as the spectra used digitally always has a finite number of data points, there is always a straight line between the data points. I.e. if a trapezium is used for area calculation between all data points in a digital image with finite step size, there is no simplification. The function does not calculate the actual area, but sets the width between every data point (i.e. the step in wavelength) to unity. This is a source of error if the wavelength step size is not equal everywhere, and it does alter in some degree for the spectra in this analysis. However, after testing, the error was found to be so small, it does not affect the normalization in a considerably degree. The most important aspect is that all spectra are normalized with respect to area calculated in the same manner.

4.2 Testing algorithm

Two techniques were implemented that had the same objective, namely to explore how the emission spectrum from different areas of the plaque varied radially. Both techniques were added as options in the program plotCorrelation.

4.2.1 Circle-method

The first technique that came to life was loosely based on the option in plotCorrelation that plots the correlation vs distance from intensity maximum/mass center. In the new option, spectra from five distances from the center is plotted, and the correlation is not taken into account. As the plaques intensity maximum and mass center vary a lot, the center is determined based on user input, as is the radii of the circles. A pixel is contributing to a circle if the distance from the center to the pixel, calculated by use of equation (3.1) and rounded to an integer, is equal to the integer radius of that particular circle.

4.2.2 Zone-method

The second technique chooses pixels in the image based on total intensity. In stead of having a certain distance from a given center, the pixels are now chosen to contribute to a zone if their total intensity lies within a certain interval. Figure 4.2 illustrates how the program works step-by-step. Figure 4.3 and 4.4 shows both circle-method and zone-method applied on two different plaques, and unveils some important differences between the two.

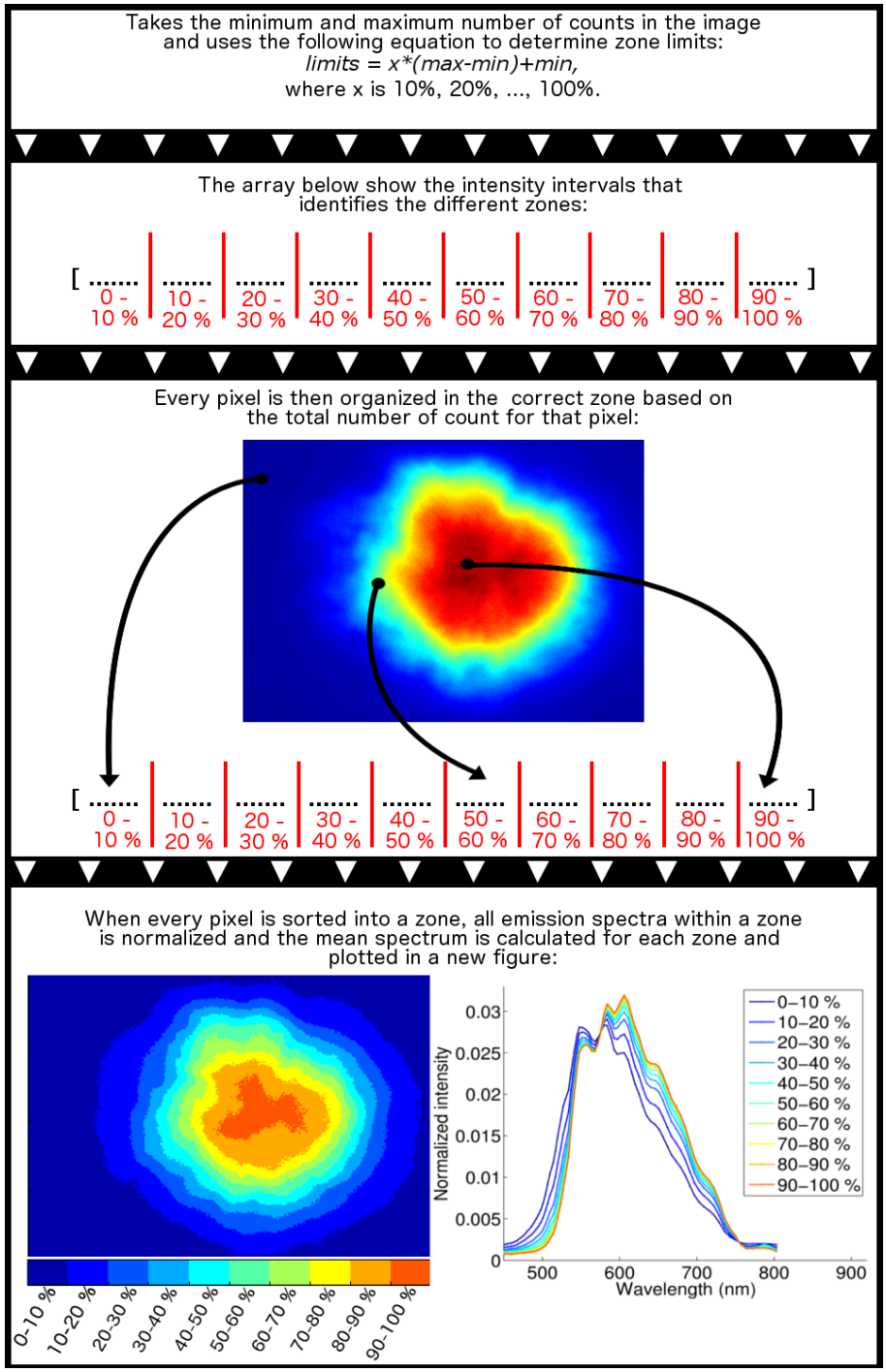

Figure 4.2: Flow chart illustrating line of action for zone-method.

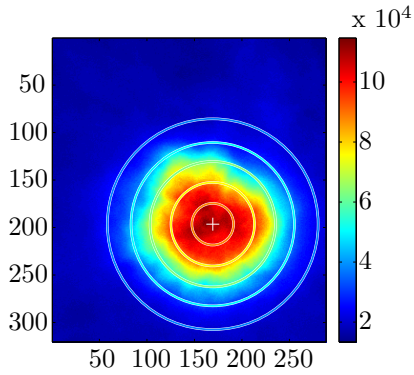

(a) Intensity image with circles. Colorbar shows number of counts.

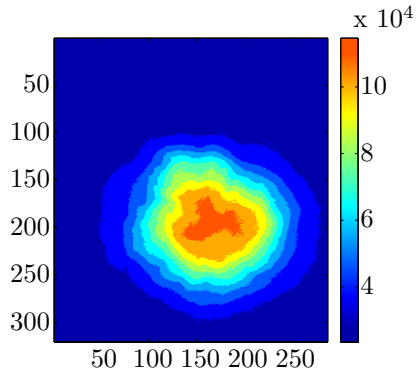

(b) Image of plaque divided into zones. Colorbar shows number of counts.

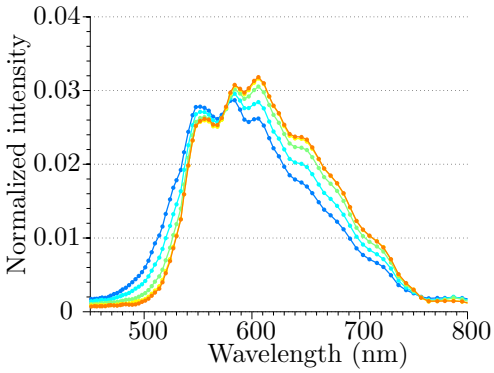

(c) Spectra from points lying on the circles seen in (a). The color of each spectrum matches the color of the circles.

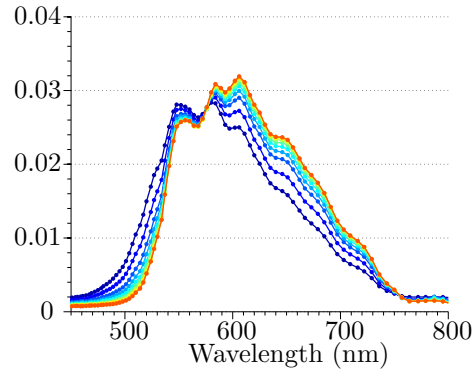

(d) Spectra from points within every zone seen in (b). The color of each spectrum matches the color of the zones.

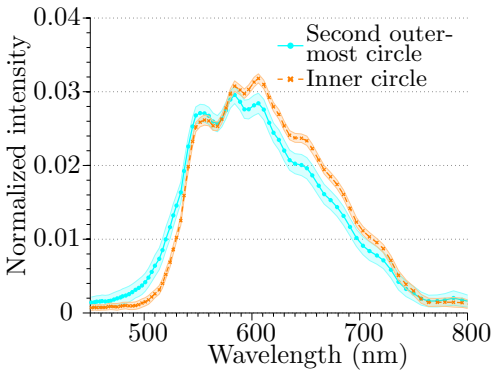

(e) Plot showing the standard deviation for every wavelength on two spectra from circle-method.

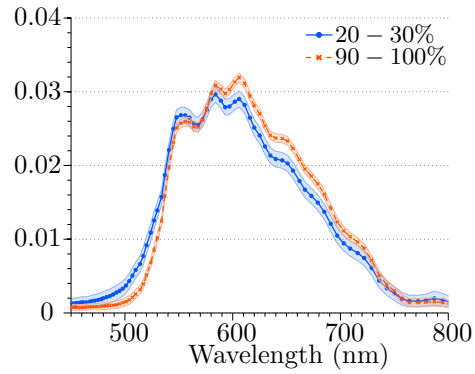

(f) Plot showing the standard deviation for every wavelength on two spectra from zone-method

Figure 4.3: Example showing usage of both circle-method and zone-method on a fairly circular plaque.

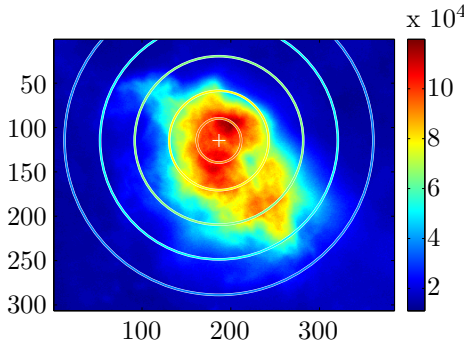

(a) Intensity image with circles. Colorbar shows number of counts.

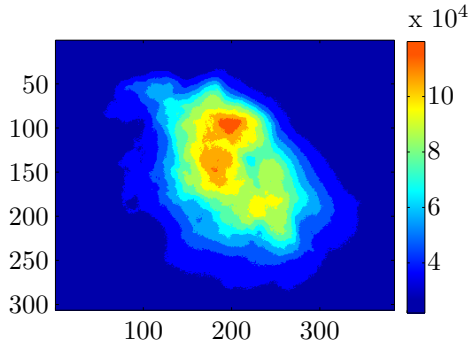

(b) Image of plaque divided into zones. Colorbar shows number of counts.

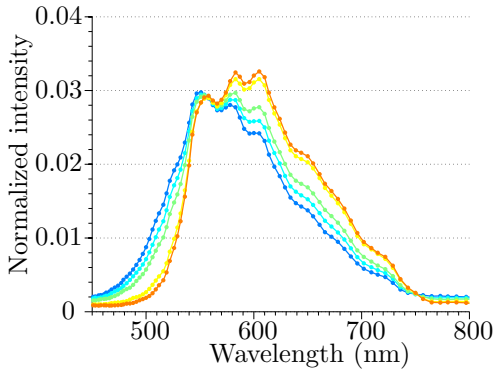

(c) Spectra from points lying on the circles seen in (a). The color of each spectrum matches the color of the circles.

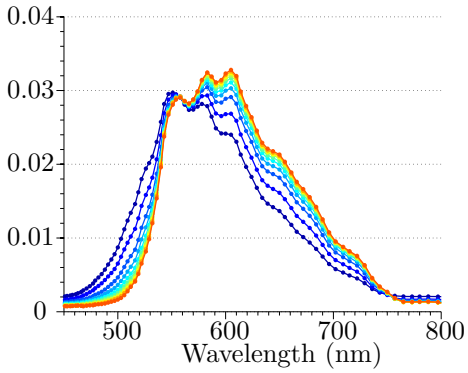

(d) Spectra from points within every zone seen in (b). The color of each spectrum matches the color of the zones.

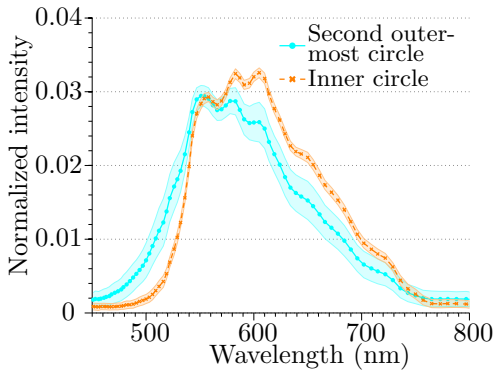

(e) Plot showing the standard deviation for every wavelength on two spectra from circle-method.

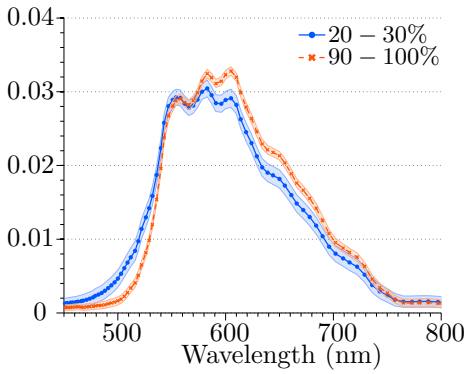

(f) Plot showing the standard deviation for every wavelength on two spectra from zone-method

Figure 4.4: Example showing usage of both circle-method and zone-method on a non-circular plaque.

4.2.3 Strengths and weaknesses of algorithms

Figure 4.3 and 4.4 show a higher standard deviation for the spectrum corresponding to the second outermost circle for the non-circular plaque relative to the circular. As one can see in figure 4.4a, the plaque's non-circularity forces the second outermost circle to cover a lot of background (i.e. low intensity areas) if it is to touch the outer edge, which gives contribution from pixels all over the image. Another bi-effect of the circle having a large radius, is that some of the points may be outside the image – and thus no contribution from these points. A lower number of contributors yield additional noise and cause the mean value to be more inaccurate with respect to expectation value, as stated in the weak law of large numbers [22]. For example, the plaque shown in figure 4.3 has approximately 500 pixels that contribute to the mean spectrum for the second outermost circle, while the corresponding zone $(20 - 30\%)$ contains over 5000 pixels as a basis for mean calculation.

A zone-method weakness is revealed if the image contains areas of slightly increased intensity in the background. A zone that seemingly covers the periphery of a plaque may then also include some background. Another point is that the image should only contain one plaque, unless one is looking for a mean spectrum for many plaques. The latter can be solved by using the cropping option in plotCorrelation.

Statistics

A method for examining hyperspectral images of this kind should be suitable for statistical purposes. Although the dataset in this report only contains a few images, other analysis may involve many hundreds, rendering it nearly impossible to do a proper analysis examining one image at the time. The resulting method should produce general results, so that they can be used for making statistics about the data set.

If the objective requires handling of many plaques, the circle-method is not suited due to multiple reasons. First of all, the vast requirement of user input makes the process lengthy. In addition, equal parameters for data acquisition is required to get meaningful statistical results, which is difficult as the radius of circles is determined by user input and will therefore not be kept constant. There is also a problem with plaques having different geometrical shape, rendering it impossible for spectra from circle-method to represent the same area. In the zone-method, zones always represent a given intensity interval, yielding more relevant statistical results.

4.3 Autofluorescence from CJD plaque

Figure 4.5 shows spectra for ten zones in a unstained plaque captured with dapi filter, i.e. the spectra represents AF for CJD plaques captured with dapi filter in the data set. As the set only contained one image of unstained plaque, it should be taken into consideration that AF spectra might vary for different plaques. The dataset did not contain an image of unstained plaque captured with green filter.

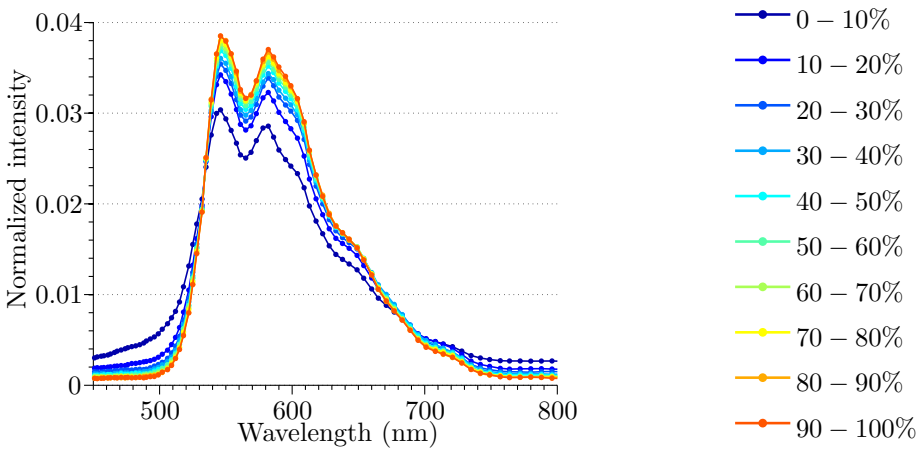

Figure 4.5: Autofluorescence of CJD plaque. Emission spectra for ten zones from unstained plaque captured with dapi filter. Peaks are located at 546 nm and 582 nm.

4.4 Correlation approach vs. linear unmixing

The work presented in this report has made use of the correlation approach to mathematically weight the spectra present in one spectrum, and not linear unmixing. The two approaches are quite similar as they both require a reference spectrum, and they are both ways to mathematically express in what degree a spectrum is present within another spectrum. The linear unmixing approach is weak for situations where a spectrum is not a linear combination of many spectra. For use like in this report, with hFTAA staining of PrP^{Sc}, the resulting emission spectrum can be a product of a chemical reaction, and is thus no linear combination of one spectrum from hFTAA and another from PrP^{Sc}. The correlation approach describes the linear relation between measured and reference spectrum. If there is no effect from the staining in a spectrum, the correlation with AF should be high, and vice versa. It does not matter in what way the staining changes the spectrum, it only matters if it is changed or not with respect to the AF spectrum.

4.5 Results from CJD plaque analysis

The dataset was organized as showed in table 4.1:

Case number	Number of plaques	PrP^{Sc} type
2	1	Type 1 M/V
7	5	Type 2 V/V
8	5	Type 2 V/V
10	4*	Type 1 M/V
11	5	Type 1 M/V
14	3	Type 2 M/V
15	5	Type 2 M/V

Table 4.1: The case numbers is in their original states as set by the university in Zürich. Every plaque in all cases is captured with two different filters. The case numbers are unique for every patient.
*Allthough the total number of plaques is four, they are organized as plaque number 1, 2, 3, 5.

4.5.1 Correlation between plaques and AF

Figure 4.6 shows correlation images for three plaques chosen to be representative for each case. The plaques displayed great variation of correlation with AF spectrum, seen as zone $90 - 100\%$ in figure 4.5. It was also a strong radially dependence on most of the plaques. Figure 4.6 shows how the plaques tend towards emitting spectra more resembling to AF at the periphery than in the center of the plaques. This effect can be understood as the hFTAA staining having more influence on the spectra originating from the central area. The result is the opposite of what was found for hFTAA-staining of amyloid β plaques in earlier LUPAS research on AD, which indicated that hFTAA stains the periphery more than the center [3].

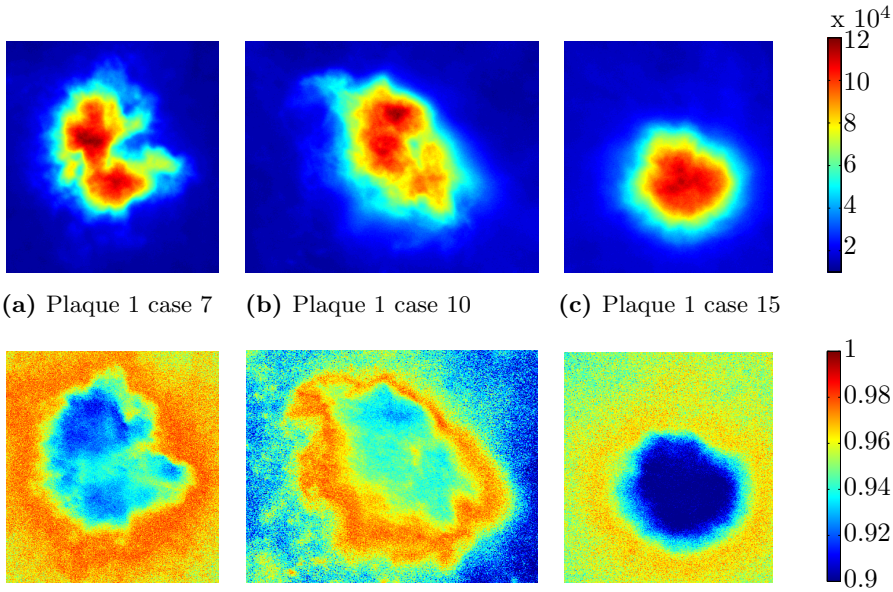

(a) Plaque 1 case 7 **(b)** Plaque 1 case 10 **(c)** Plaque 1 case 15

(e) Correlation between (a) and AF **(f)** Correlation between (b) and AF **(g)** Correlation between and RS

Figure 4.6: (a)-(c) shows intensity maps for hyperspectral images of three different plaques. (d)-(f) shows the correlation between the dapi filtered image and the dapi filtered AF (see figure 4.5). The top color bar shows the intensity, and the lower color bar shows the correlation. Notice how the correlation increases as the distance from the center of the plaques increases.

4.5.2 Radial distribution of correlation

plotCorrelation has the option to show the correlation as a function of distance from intensity maximum (center). The function has data points for every radius rounded to an integer (calculated in pixels), where maximum radius is the pixel farthest off the center. To make the data useful for statistical work, the radii were normalized and resampled to 30 points from 0 to 1. When normalized and resampled, the mean correlation pr distance from center with standard deviation can be found for each case. Figure 4.7 shows the mean correlation and standard deviation as a function of normalized distance from the center for all plaques within three cases.

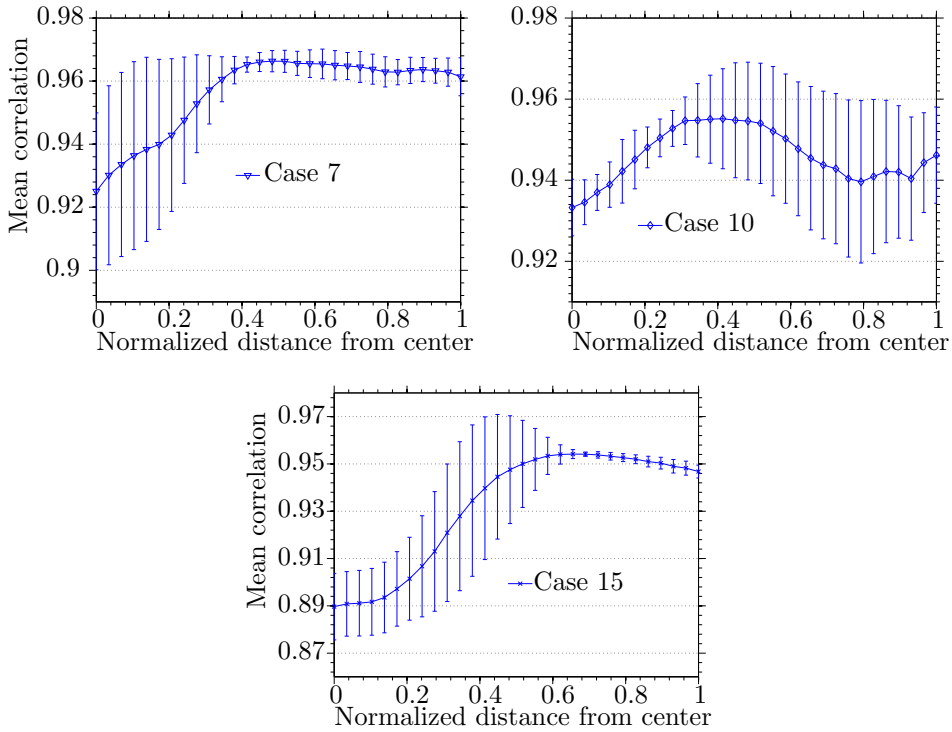

Figure 4.7: The mean correlation and standard deviation for all plaques within case 7, 10 and 15 as a function of normalized distance from intensity maximum. Case 10 contains three plaques, while 7 and 15 has five.

The correlation with AF increases as the distance increases for all three cases. As previously stated, this indicates that the hFTAA staining influences the center most for all plaques in the three cases, owing to the fact that correlation with the non-stained plaque is highest at the periphery. This can only be stated with the reservation of the un-stained plaque has a emission spectrum representative for the autofluorescence of CJD plaques. As figure 4.7 shows, the standard deviation varies massively for the different cases. This effect can not be seen as only a variation in correlation at certain regions of the plaque. The program is written in such a way that it is most reliable on circular plaques, as it choses the pixel with maximum intensity as center, and gets the spectra as a function of distance from this center. This yields high uncertainty and variation in correlation at large distances for plaques with irregular shape and many different areas of high intensity.

The acquisition of spectra in the circle-method is loosely based on this procedure, which is why their weaknesses are more or less the same. For example, case 10 consists of three differently shaped plaques (plaque 1, 2 and 5 in case 10, see appendix 1). Because they at large distances away from the center will represent different areas of the plaque, the standard deviation is high. On the other hand, case 15 contains five more or less circular plaques located at the center of the image,

yielding all correlation values far away from the center to represent the transition from periphery to background, and therefore the low standard deviation.

A statistical problem arises when the distance is normalized to be from 0 to 1. Ideally, one would like a certain distance to represent the periphery of the plaque, another distance to be the background, and so on. This would require the crops of the images to be done in such a way that each plaque occupies the same amount of area, and the plaque should be centered. In the data presented in this report, the cropping was already done, so small variations will give a higher standard deviation seen in figure 4.7. However, the effect of non-circularity is a greater source of inaccuracy for this procedure. Note that the standard deviation shown in 4.7 concerns the variation between the different plaques, i.e. it is about uncertainty in statistics. Non-circular plaques will also cause a high standard deviation in the correlation vs. distance-plot for one single plaque, which in turn yields high standard deviation in statistical use.

4.5.3 Radial distribution of ES

Figure 4.8 shows how the mean emission spectrum for three cases with both filters varies radially. The calculation of a mean spectrum for a case was done by taking the mean normalized intensity value for every wavelength value. The normalization is done with respect to the area under the curve, and prevents the total intensity of the hyperspectral image to affect the result. Figure 4.9 shows the standard deviation for the mean spectra of zone $20-30\%$ and $90-100\%$ seen in figure 4.8.

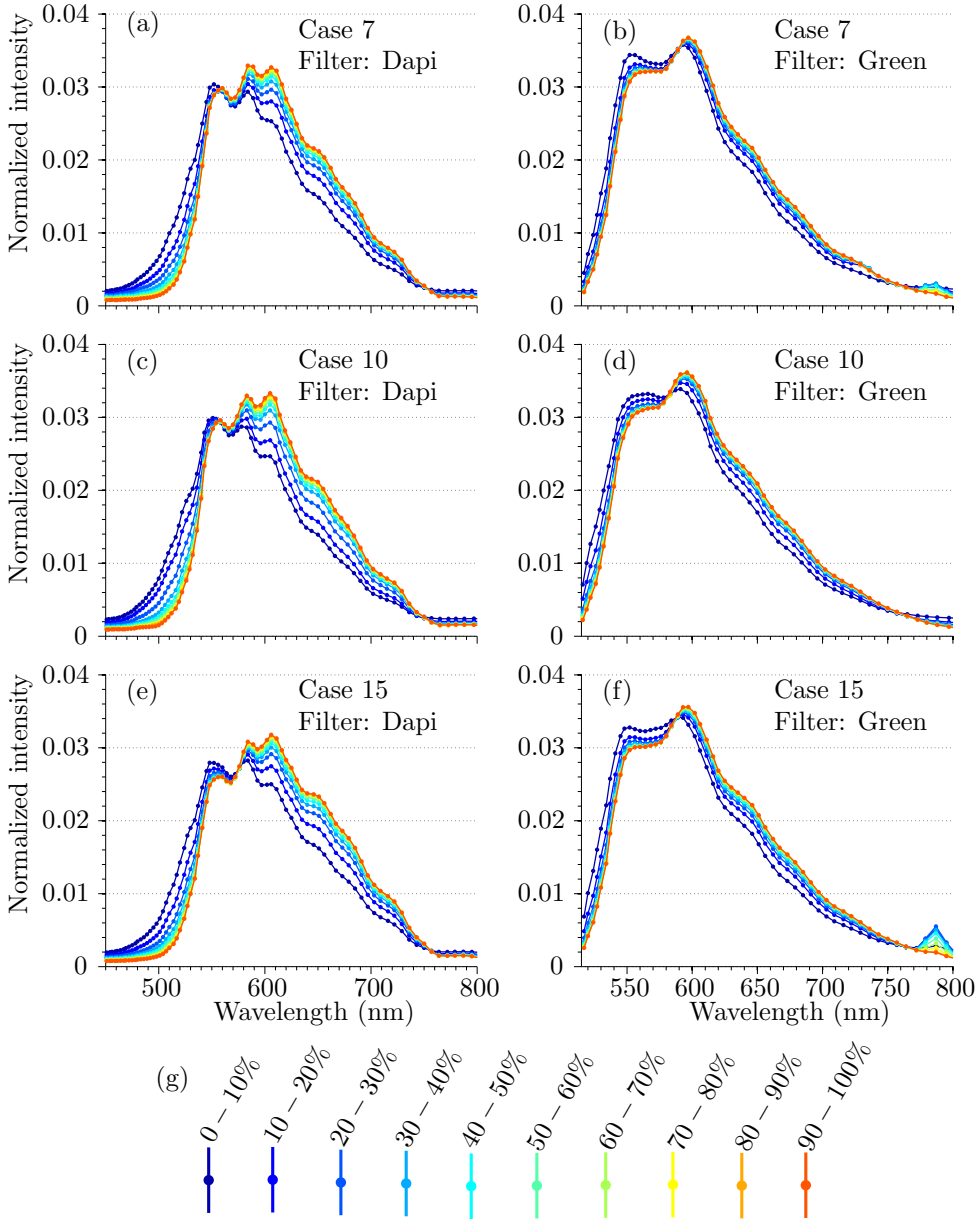

Figure 4.8: Plots showing mean emission spectra for each zone in all plaques in one case. (g) shows legend for (a) - (f). Peaks for dapi filtered plots are at 555 nm, 584 nm and 606 nm. Peaks for green filtered plots are at 555 nm and 590 nm.

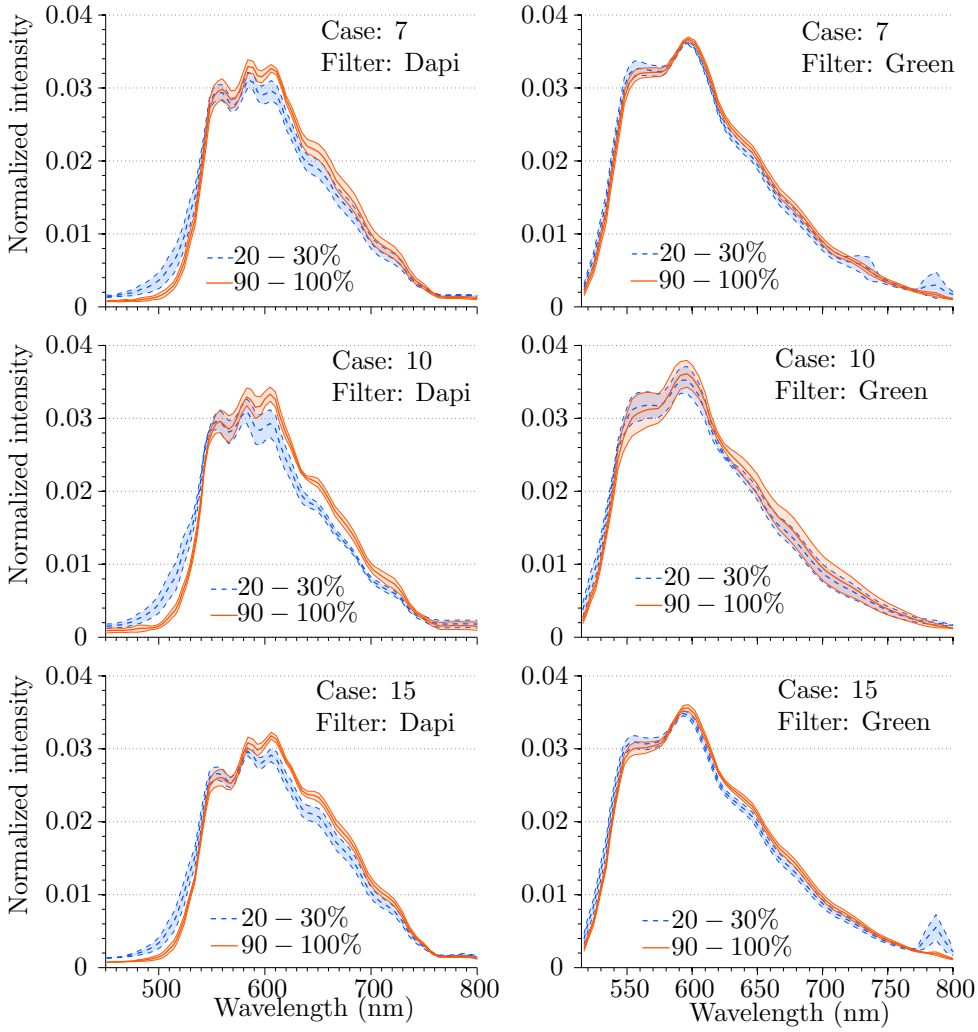

Figure 4.9: Plots showing the for lines 20 – 30% and 90 – 100% in figure 4.8. The shaded outlines represent the standard deviation for the mean spectrum of all plaques in three different cases.

Figure 4.8 displays a red shift for both dapi and green filtered spectra as the zones approaches the center. For the dapi filter spectra, a new maxima at 606 nm arises. Dapi spectra are more red shifted, and has three local maxima compared to two in green spectra. The radial dependency is therefore more evident for dapi spectra. The standard deviation seen in figure 4.9 can in general be said to be low. There is possible to see a slightly increment for case 10, especially for green filter. Some of the reason for this can possibly be traced back to the number of plaques involved in the case. As the plot is a mean of three plaques, compared to

five plaques for case 7 and case 15, a deviation in the plaque's emission spectrum[1] will affect the standard deviation in a higher degree.

4.6 Sources of error

4.6.1 pH change during preparation

A discussion within the group of the collaborators within the LUPAS project revealed a possible source of error because the sections were decontaminated with 2M NaOH. If the nail polish sealing is leaky, NaOH could access the tissue. A pH change could massively modify the spectra. As can be seen in appendix 5, a lot of the correlation images looks completely "red", meaning the correlation with AF reference is close to 1 over the entire image. For this reason, results for the "red" images is not included in this report. The excluded plaques are all plaques in case 2, 8, 11 and 14, and plaque 3 in case 10.

4.6.2 Limited number of AF references

The dataset contained only one image of unstained plaque. It can not be guaranteed that it is a representative AF spectrum for the center of PrP^{Sc}, as one can not rule out sources of error like NaOH leakage.

[1] A deviation could originate from for instance sample preparation, prion type heterogeneity, capturing process etc.

Chapter 5

Summary and Conclusion

A dataset containing 56 hyperspectral images of hFTAA stained PrP^{Sc} plaques from CJD infected human brain tissue was analyzed, captured with two different filters (dapi and green). To get an overview, the MatLab program plotCorrelation [4] (that calculates the correlation coefficient between the emission spectrum for every pixel and a reference spectrum) was used on every image with AF as reference spectrum. The correlation images revealed a strong radial dependence for the emission spectrum.

To examine what happened to the emission spectrum as the distance from the center of the plaque was increased, two new programs were implemented and added as an option to plotCorrelation. The underlying idea was to make a program that took a hyperspectral image as input and plotted a number of spectrums dependent on the distance from a chosen centre. The number of plots should be so low that they could be plotted in one 2D coordinate system and still be separable to the eye. One program was based on pixels lying on a circle around a given centre, and another based on dividing the image into zones based on total intensity.

The program using circles required a lot of user input and did not contain as many pixels for mean spectrum calculation as the program based on zone classification. The zone-method also gave more reliable results for non-circular plaques, and did not require any user input. For this reason the zone-method was preferred in further analysis.

It was revealed that close to the center of the plaques, a peak at 606 nm appeared for the dapi filtered images, and a distinct red shift appeared for both dapi and green filtered images for spectra extracted from the periphery to the center of the plaques. The peak at 606 nm was absent for a unstained sample present in the dataset. This implied that the hFTAA staining of PrP^{Sc} plaques was most pronounced in the center, which is the opposite of what was found in earlier research on hFTAA staining of Amyloid-β plaques from AD, that concluded with hFTAA staining being most evident in the periphery of the plaques [3].

Bibliography

[1] Ignazio Cali, Rudolph Castellani, Jue Yuan, Amer Al-Shekhlee, Mark L. Cohen, Xiangzhu Xiao, Francisco J. Moleres, Piero Parchi, Wen-Quan Zou, and Pierluigi Gambetti. Classification of sporadic creutzfeldtjakob disease revisited. *Brain*, 129(9):2266–2277, 2006.

[2] dr. Rainer Wegerhoff, Dr. Olaf Weidlich, and Dr. Manfred Kässens. Basics of light microscopy & imaging (special edition of imaging & microscopy). Publised by GIT VERLAG Gmbh & Co. KG.

[3] Pål Gunnar Ellingsen, Sofie Nyström, Nina Kristine Reitan, and Mikael Lindgren. Spectral correlation analysis of amyloid β plaque inhomogeneity from double staining experiments. Unpublished.

[4] Pål Gunnar Ellingsen, Nina Kristine Reitan, Brede Dille Pedersen, and Mikael Lindgren. Hyperspectral analysis using the correlation between image and reference. *Journal of Biomedical Optics*, 18(2):020501–020501, 2013.

[5] Yuval Garini, Ian T. Young, and George McNamara. Spectral imaging: Principles and applications. *Cytometry part A*, 69A(8):735 – 747, 2006.

[6] Mark W. Head, Tristan J. R. Bunn, Matthew T. Bishop, Victoria McLoughlin, Suzanne Lowrie, Clive S. McKimmie, Michelle C. Williams, Linda McCardle, Jan MacKenzie, Richard Knight, Robert G. Will, and James W. Ironside. Prion protein heterogeneity in sporadic but not variant creutzfeldtjakob disease: U.k. cases 19912002. *Annals of Neurology*, 55(6):851–859, 2004.

[7] Science in Your Eyes. Fluorescence microscopy - a brief explanation. `http://www.scienceinyoureyes.com/index.php?id=79`.

[8] David Landgrebe. On information extraction principles for hyperspectral data, a white paper. `http://www.daba.lv/grozs/Datorlietas/Geog5028/TIS_PRG/MultiSpecWin32/tutorial/whitepaper.pdf`.

[9] Rusty Lansford, Gregory Bearman, and Scott E. Fraser. Resolution of multiple green fluorescent protein color variants and dyes using two-photon microscopy and imaging spectroscopy. *Journal of Biomedical Optics*, 6(3):311–318, 2001.

[10] Annenberg learner. Physics for the 21st century, unit 9, section 4: Proteins. `http://www.learner.org/courses/physics/unit/text.html?unit=9&secNum=4`.

[11] Barry R Masters. *History of the Optical Microscope in Cell Biology and Medicine*. John Wiley & Sons, Ltd, 2001.

[12] Mathworks. Trapz documentation. `http://www.mathworks.se/help/matlab/ref/trapz.html`.

[13] MATLAB. *version 8.0.0.783 (R2012b)*. The MathWorks Inc., Natick, Massachusetts, 2012.

[14] Kohtaro Miyazawa, Kaitlin Emmerling, and Laura Manuelidis. Replication and spread of cjd, kuru and scrapie agents in vivo and in cell culture. *Virulence*, 2(3):188 – 199, 2011.

[15] M. P. Morrissey and E. I. Shakhnovich. Evidence for the role of prpc helix 1 in the hydrophilic seeding of prion aggregates. *Proceedings of the National Academy of Sciences*, 96(20):11293–11298, 1999.

[16] Karah E Nazor, Franziska Kuhn, Tanya Seward, Mike Green, Daniel Zwald, Mario Prro, Jaqueline Schmid, Karin Biffiger, Aisling M Power, Bruno Oesch, Alex J Raeber, and Glenn C Telling. Immunodetection of disease-associated mutant prp, which accelerates disease in gss transgenic mice. *The Embo Journal*, 24(13):2472 – 2480, 2005.

[17] Parchi P, Castellani R, Capellari S, Ghetti B, Young K, Chen SG, Farlow M, Dickson DW, Sima AA, Trojanowski JQ, Petersen RB, and Gambetti P. Molecular basis of phenotypic variability in sporadic creutzfeldt-jakob disease. *Ann. Neurol.*, 39(6):767 – 778, 1996.

[18] K M Pan, M Baldwin, J Nguyen, M Gasset, A Serban, D Groth, I Mehlhorn, Z Huang, R J Fletterick, and F E Cohen. Conversion of alpha-helices into beta-sheets features in the formation of the scrapie prion proteins. *PNAS*, 90(23):10962 – 10966, 1993.

[19] Piero Parchi, Rosaria Strammiello, Silvio Notari, Armin Giese, Jan P. M. Langeveld, Anna Ladogana, Inga Zerr, Federico Roncaroli, Patrich Cras, Bernardino Ghetti, Maurizio Pocchiari, Hans Kretzschmar, and Sabina Capellari. Incidence and spectrum of sporadic creutzfeldtjakob disease variants with mixed phenotype and co-occurrence of prp^{sc} types: an updated classification. *Acta. Neuropathol.*, 118(5):659 – 671, 2009.

[20] Jiri G. Safar. Molecular pathogenesis of sporadic prion diseases in man. *Prion*, 6(2):108 – 115, 2012.

[21] Gaby Schoch, Harald Seeger, Julien Bogousslavsky, Markus Tolnay, Robert Charles Janzer, Adriano Aguzzi, and Markus Glatzel. Analysis of prion strains by prp^{sc} profiling in sporadic creutzfeldtjakob disease. *PLoS Med.*, 3(2):e14, 2006.

[22] Alan Stuart and J. Keith Ord. *Distribution Theory*, volume 1 of *Kendall's Advanced Theory of Statistics*. Edward Arnold Publishers Ltd., sixth edition, 1994.

[23] Gerard A. Venema. *Foundations of geometry*. Pearson education, 2006.

[24] Ronald E. Walpole, Raymond H. Myers, Sharon L. Myers, and Keying Ye. *Probability & Statistics for Engineers & Scientist*. Pearson Education, Upper Saddle River, NJ 07458, USA, 8 edition, 2007.

[25] Bettina M. Wegenast-Braun, Angelos Skodras, Gonca Bayraktar, Jasmin Mahler, Sarah K. Fritschi, Therése Klingstedt, Jeffrey J. Mason, Per Hammarström, K. Peter R. Nilsson, Christian Liebig, and Mathias Jucker. Spectral discrimination of cerebral amyloid lesions after peripheral application of luminescent conjugated oligothiophenes. *The American Journal of Pathology*, 181(6):1953 – 1960, 2012.

[26] Laura Westergard, Heather M. Christensen, and David A. Harris. The cellular prion protein (prp^{c}): Its physiological function and role in disease. *Biochimica et Biophysica Acta (BBA) - Molecular Basis of Disease*, 1772(6):629 – 644, 2007.

[27] Holger Wille, Melissa D. Michelitsch, Vincent Gunebaut, Surachai Supattapone, Ana Serban, Fred E. Cohen, David A. Agard, and Stanley B. Prusiner. Structural studies of the scrapie prion protein by electron crystallography. *PNAS*, 99(6):629 – 644, 2002.

[28] Zeiss. Overview filter sets. `https://www.micro-shop.zeiss.com/?s=210968587252b8&l=en&p=us&f=f&a=f`.

[29] Timo Zimmermann, Jens Rietdorf, and Rainer Pepperkok. Spectral imaging and its applications in live cell microscopy. *FEBS letters*, 546(1):87 – 92, 2003.

Appendix A: Complete list of all plaques including correlation with AF

This is an overview of the hyperspectral image's correlation with spectrum from the center of the unstained plaque. The right columns is the intensity images of the plaques, and the right is the correlation. The center mean stated in all captions for intensity images is the mean intensity in the $90 - 100\%$ zone (the highest 10% of intensity area).

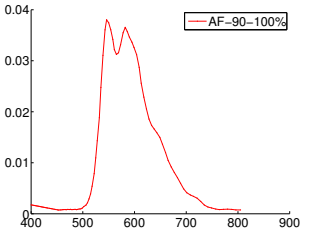

(1.1) Reference spectrum (AF)

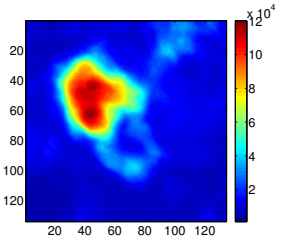

(1.2) AF. Center mean: 118576

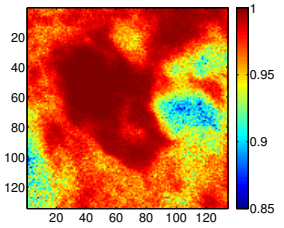

(1.3) correlation with AF

Figure 1: Unstained plaque. Hyperspectral images in left column, and correlation with AF in right column.

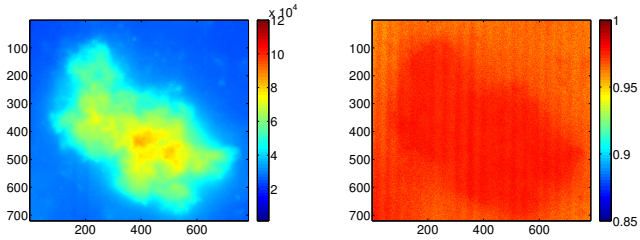

(2.1) 2-1. Center mean: 87696 **(2.2)** correlation with AF

Figure 2: Case 2. Hyperspectral images in left column, and correlation with AF in right column.

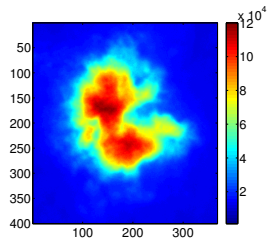

(3.1) 7-1. Center mean: 119801

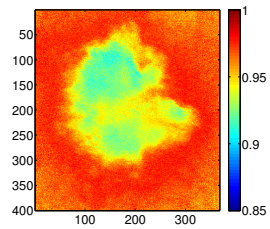

(3.2) correlation with AF

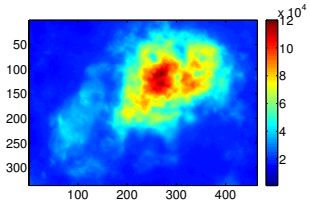

(3.3) 7-2. Center mean: 119876

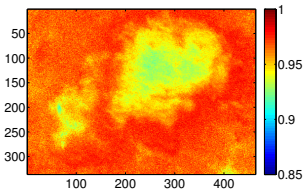

(3.4) correlation with AF

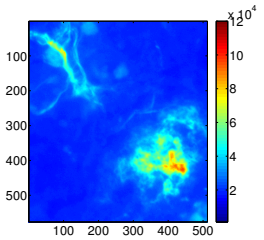

(3.5) 7-3. Center mean: 99229

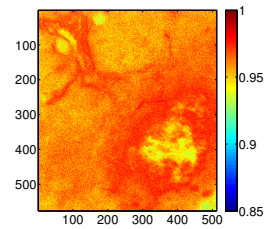

(3.6) correlation with AF

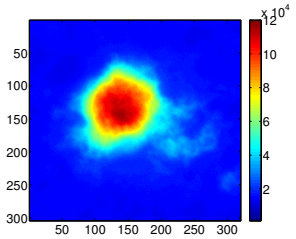

(3.7) 7-4. Center mean: 117263

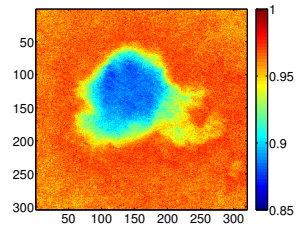

(3.8) correlation with AF

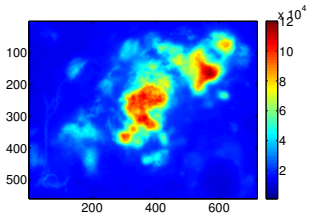

(3.9) 7-5. Center mean: 117836

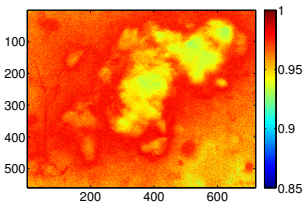

(3.10) correlation with AF

Figure 3: Case 7. Hyperspectral images in left column, and correlation with AF in right column.

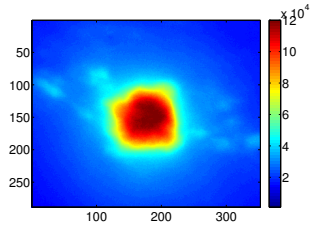

(4.1) 8-1. Center mean: 122806

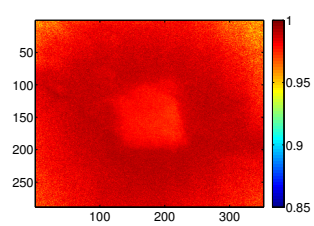

(4.2) correlation with AF

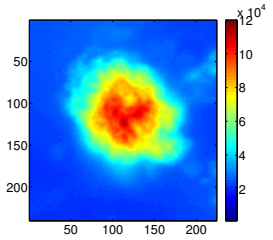

(4.3) 8-2. Center mean: 113046

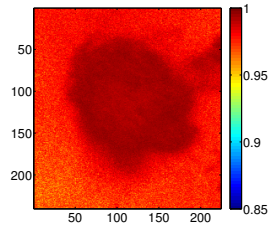

(4.4) correlation with AF

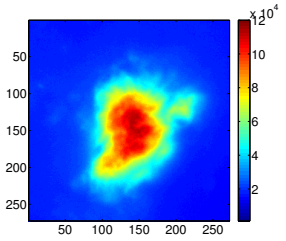

(4.5) 8-3. Center mean: 114811

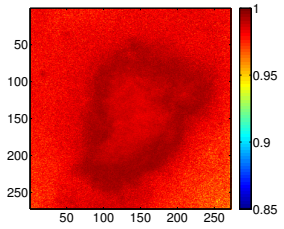

(4.6) correlation with AF

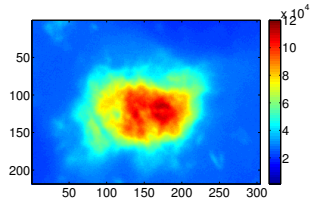

(4.7) 8-4. Center mean: 114347

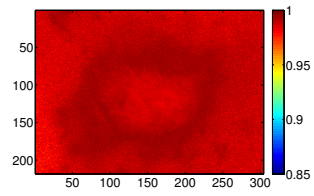

(4.8) correlation with AF

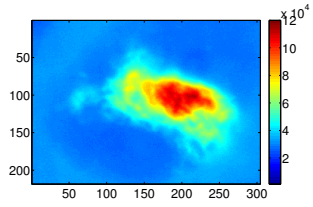

(4.9) 8-5. Center mean: 115239

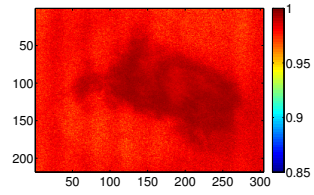

(4.10) correlation with AF

Figure 4: Case 8. Hyperspectral images in left column, and correlation with AF in right column.

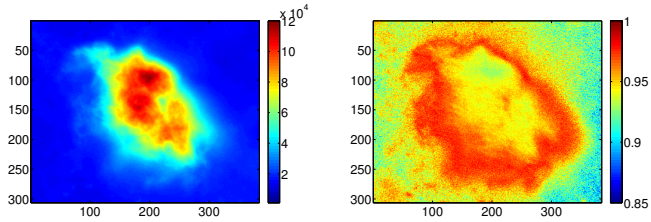

(5.1) 10-1. Center mean: **(5.2)** correlation with AF 119847

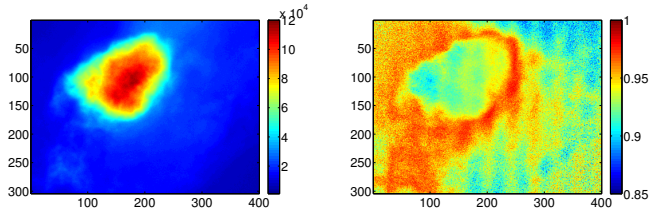

(5.3) 10-2. Center mean: **(5.4)** correlation with AF 116077

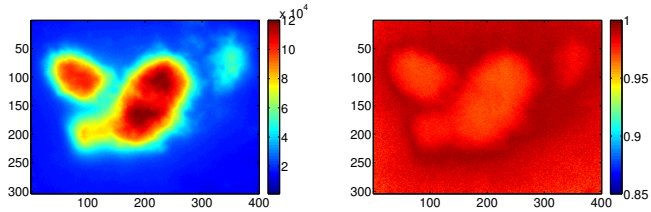

(5.5) 10-3. Center mean: **(5.6)** correlation with AF 121419

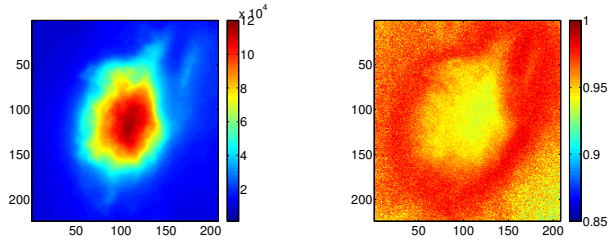

(5.7) 10-5. Center mean: **(5.8)** correlation with AF 117384

Figure 5: Case 10. Hyperspectral images in left column, and correlation with AF in right column.

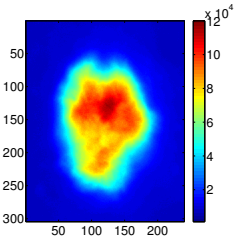

(6.1) 11-1. Center mean: 116868

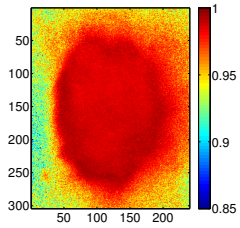

(6.2) correlation with AF

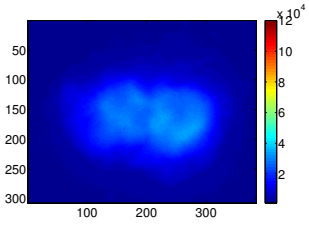

(6.3) 11-2. Center mean: 34987

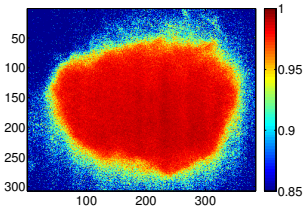

(6.4) correlation with AF

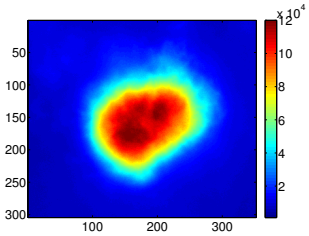

(6.5) 11-3. Center mean: 123549

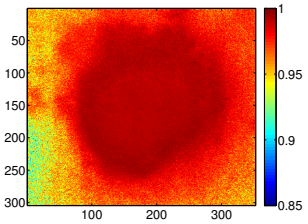

(6.6) correlation with AF

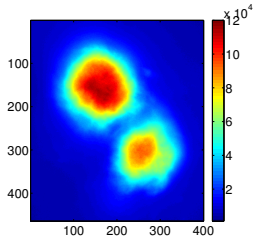

(6.7) 11-4. Center mean: 117106

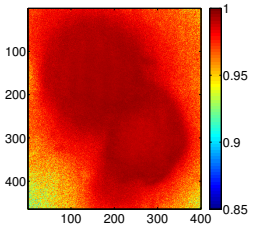

(6.8) correlation with AF

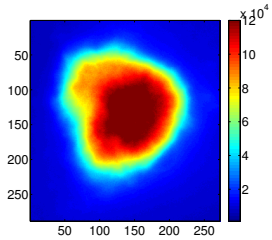

(6.9) 11-5. Center mean: 135620

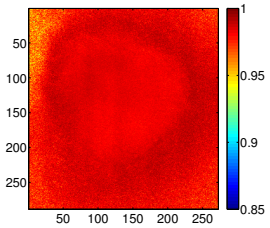

(6.10) correlation with AF

Figure 6: Case 11. Hyperspectral images in left column, and correlation with AF in right column.

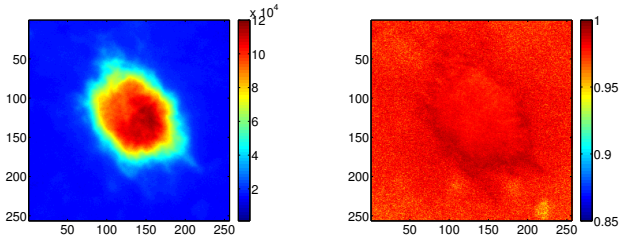

(7.1) 14-1. Center mean: **(7.2)** correlation with AF 116923

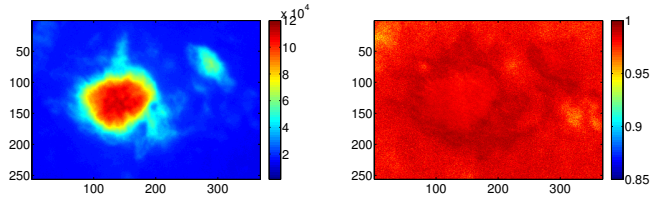

(7.3) 14-2. Center mean: **(7.4)** correlation with AF 113003

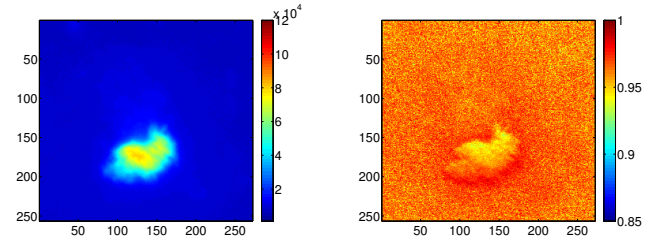

(7.5) 14-3. Center mean: **(7.6)** correlation with AF 81243

Figure 7: Case 14. Hyperspectral images in left column, and correlation with AF in right column.

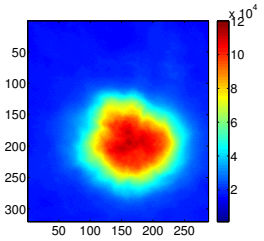

(8.1) 15-1. Center mean: 114667

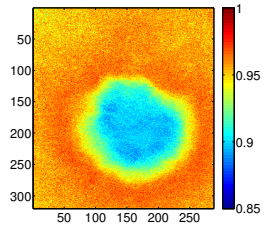

(8.2) correlation with AF

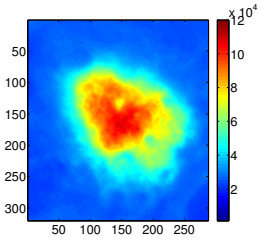

(8.3) 15-2. Center mean: 110348

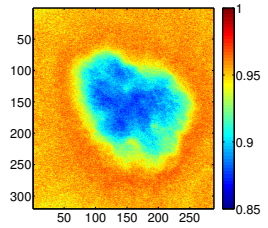

(8.4) correlation with AF

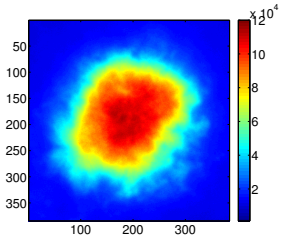

(8.5) 15-3. Center mean: 115605

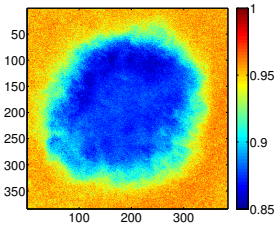

(8.6) correlation with AF

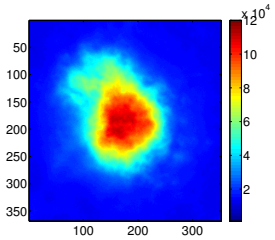

(8.7) 15-4. Center mean: 113338

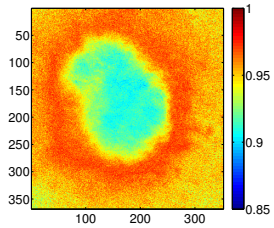

(8.8) correlation with AF

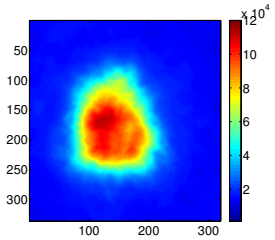

(8.9) 15-5. Center mean: 113425

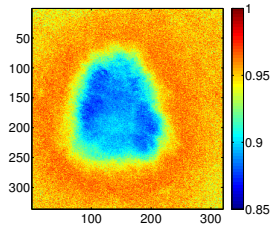

(8.10) correlation with AF

Figure 8: Case 15. Hyperspectral images in left column, and correlation with AF in right column.

Appendix B: Program code for zone-method

```
if args.zones
    xStep=0.1:0.1:1;
    %xStep = [0.6 0.65:0.02:1]; %alternative xStep
    %xStep defines which percentage of the intensity is placed in what
    %zone. Another vector can also be used, as long as xStep(1)>0 and
    %xStep(end)==1.

    img = squeeze(sum(A,3));
    %img=B.corr; %alternative img
    zones=xStep*(max(max(img))-min(min(img)))+min(min(img));

    cm = jet(length(xStep)); %creating the colormap
    cimage=zeros(size(img)); %cimage is the image divided into zones
    zSpec=zeros((length(xStep)),size(A,3)); %zSpec contains all the spectra from the zones
    At = trapz(A,3);
    Anorm = zeros(size(A));
    for i=1:size(A,3)
        Anorm(:,:,i) = A(:,:,i)./At; %Normalizing the spectrum for every pixel in the image
    end
    if args.plot
        figure(figN);
        clf;
        hold on
    end
    nspec=cell(1,length(xStep));
    B(1).zStd=zeros(length(xStep),length(wave));
    B(1).zStdd=zeros(length(xStep),length(wave));
    for i=1:length(xStep)
        if i==1
            boolImg=(zones(i)>=img);
        elseif i==length(xStep)
            boolImg=(zones(i-1)<img);
        else
            boolImg=(zones(i-1)<img)&(img<=zones(i));
        end
        cimage(boolImg)=zones(i);
        tmpImg = Anorm;
        tmpImg(repmat(~boolImg,[1 1 size(tmpImg,3)])) = NaN;
        zSpec((i),:)=nanmean(nanmean(tmpImg));

        for j=1:length(wave)
            tmpi = tmpImg(:,:,j);
            B(1).zStd(i,j) = std(tmpi(isfinite(tmpi)));
        end

        if args.mNorm
            nspec{i} = normalize(zSpec(i,:),'m');
        else
```

```
49              nspec{i} = normalize(zSpec(i,:),'a');
50          end
51
52          if args.plot
53              plot(wave,nspec{i},'-','color',cm(i,:),'LineWidth',1)
54          end
55      end
56      B(1).zoneSpec.spec=nspec;
57      B(1).zoneSpec.legend = zones;
58      if args.plot
59          hold off
60          figN=figN+1;
61          figure(figN);
62          clf;
63          imagesc(cimage)
64          axis image
65          colormap(cm); %Plotting cimage with the same colormap as
                the reference spectras.
66          colorbar;
67          figN=figN+1;
68      end
69
70      B(1).zoneIm = cimage;
71  end
```

Appendix C: Program code for circle-method

```
if args.circles
    if ~args.input
        warning('Circle analysis requires user input');
    end
    n=5; %number of circles
    if args.plot
        figure(figN);
        figN=figN+1;
        clf;
        img=squeeze(sum(A,3));
        imagesc(img);
        hold on
        axis image
        title(['First choose the center, then choose ',num2str(n),
            ' desired radii'])
        disp(['First choose the center, then choose ',num2str(n),'
             desired radii']);
        center=ginput(1);
        plot(center(1),center(2),'+w','MarkerSize',15)

        X=zeros(1,n);
        Y=zeros(1,n);
        [X,Y]=ginput(n);
    else
        error('Cannot turn off plots and use circle analysis')
    end

    cm=jet(n);%creating the colormap needed.

    %Calculating the radii
    for i=1:n
        R(i)=int32(sqrt((center(1)-X(i)).^2+(center(2)-Y(i)).^2));
        viscircles(center,R(i),'EdgeColor',cm(i,:))
    end

    AA=A(:,:,1);
    C=cellfun(@(n) 1:n, num2cell(size(AA)),'uniformoutput',0); %
        Constructs two
    % vectors, from 1 til length of y or x axis in a cell array
    [C{:}]=ndgrid(C{:}); % Makes a ndgrids of the cell elemets
    C=cellfun(@(x) x(:), C,'uniformoutput',0); % Arranges the
        cells into
    % vectors
    C=[C{:}]; % Converts the cell elements to an array
    cmc=bsxfun(@minus,C,center(1,:)); % subtracts of the center

    if args.plot
        figure(figN)
        figN=figN+1;
        clf;
        hold on
        title('Plot showing the average reference spectra for each
             ring')
```

```
49      end
50      cSpec=zeros(size(A,3),n);
51      At = trapz(A,3);
52      Anorm = zeros(size(A));
53      for i=1:size(A,3)
54          Anorm(:,:,i) = A(:,:,i)./At; %Normalizing the spectrum for
                every pixel in the image
55      end
56      for j=1:n
57          %cmcPos = find(sqrt(cmc(:,1).^2+cmc(:,2).^2)<(R(j)+0.5) &
                sqrt(cmc(:,1).^2+cmc(:,2).^2)>(R(j)-0.5));%Finner
                interessante posisjoner i arrayen cmc
58          cmcPos = find(int32(sqrt(cmc(:,1).^2+cmc(:,2).^2))==(R(j))
                );
59          Bpos = C(cmcPos,:); %Finner relevante posisjoner i
                matrisen C
60          size(Bpos)
61          for k=1:size(A,3) %Henter referansespektraene og tar
                gjennomsnittet
62              tmpValues=zeros(size(Bpos,1),1);
63              for l=1:size(Bpos,1)
64                  tmpValues(l) = Anorm(Bpos(l,2),Bpos(l,1),k);
65              end
66              cSpec(k,j)=mean(tmpValues);
67              cSdev(k,j)=std(tmpValues);
68          end
69
70          if args.mNorm
71              nCspec{j} = normalize(cSpec(:,j),'m');
72          else
73              nCspec{j} = normalize(cSpec(:,j),'a');
74          end
75
76          if args.plot
77              plot(wave,nCspec{j},'-','color',cm(j,:),'LineWidth',1)
78          end
79      end
80      B(1).circleSpec.spec=cSpec;
81      B(1).circleSpec.std=cSdev;
82  end
```